Redox Biology 49 (2022) 102219

Contents lists available at ScienceDirect

Redox Biology

journal homepage: www.elsevier.com/locate/redox

A new FGF1 variant protects against adriamycin-induced cardiotoxicity via modulating p53 activity

Mengjie Xiao [a], Yufeng Tang [b], Jie Wang (a) [a], Guangping Lu [a], Jianlou Niu [c], Jie Wang (b) [a], Jiahao Li [a], Qingbo Liu [a], Zhaoyun Wang [d], Zhifeng Huang [c], Yuanfang Guo [a], Ting Gao [a], Xiaohui Zhang [a], Shouwei Yue [e], Junlian Gu [a,*]

[a] School of Nursing and Rehabilitation, Cheeloo College of Medicine, Shandong University, Jinan, Shandong, 250012, China
[b] Department of Orthopedic Surgery, The First Affiliated Hospital of Shandong First Medical University, Jinan, Shandong, 250014, China
[c] School of Pharmaceutical Science, Wenzhou Medical University, Wenzhou, Zhejiang, 325035, China
[d] Department of Neurosurgical Intensive Care Unit & Emergency Neurosurgery, Qilu Hospital of Shandong University, Jinan, Shandong, 250012, China
[e] Rehabilitation Center, Qilu Hospital, Cheelo College of Medicine, Shandong University, Jinan, Shandong, 250012, China

ARTICLE INFO

Keywords:
Adriamycin
Cardiotoxicity
FGF1 variant
Oxidative stress
Apoptosis

ABSTRACT

A cumulative and progressively developing cardiomyopathy induced by adriamycin (ADR)-based chemotherapy is a major obstacle for its clinical application. However, there is a lack of safe and effective method to protect against ADR-induced cardiotoxicity. Here, we found that mRNA and protein levels of FGF1 were decreased in ADR-treated mice, primary cardiomyocytes and H9c2 cells, suggesting the potential effect of FGF1 to protect against ADR-induced cardiotoxicity. Then, we showed that treatment with a FGF1 variant ($FGF1^{\Delta HBS}$) with reduced proliferative potency significantly prevented ADR-induced cardiac dysfunction as well as ADR-associated cardiac inflammation, fibrosis, and hypertrophy. The mechanistic study revealed that apoptosis and oxidative stress, the two vital pathological factors in ADR-induced cardiotoxicity, were largely alleviated by $FGF1^{\Delta HBS}$ treatment. Furthermore, the inhibitory effects of $FGF1^{\Delta HBS}$ on ADR-induced apoptosis and oxidative stress were regulated by decreasing p53 activity through upregulation of Sirt1-mediated p53 deacetylation and enhancement of murine double minute 2 (MDM2)-mediated p53 ubiquitination. Upregulation of p53 expression or cardiac specific-*Sirt1* knockout (*Sirt1*-CKO) almost completely abolished $FGF1^{\Delta HBS}$-induced protective effects in cardiomyocytes. Based on these findings, we suggest that $FGF1^{\Delta HBS}$ may be a potential therapeutic agent against ADR-induced cardiotoxicity.

1. Introduction

Adriamycin (ADR), also known as doxorubicin (DOX), is one of the most highly prescribed anthracyclines due to its broad spectrum of therapeutic efficacy. Anthracycline-based chemotherapy can lead to the development of a cumulative and progressively cardiomyopathy, which can result in heart failure and even death in patients [1]. Understanding the primary mechanism in ADR-induced cardiotoxicity is essential to avoid the obstacles that so dramatically limit the clinical success of this essential anticancer chemotherapy. In fact, multiple factors have been proved to be involved in ADR-related cardiotoxicity, of which myocardial cell apoptosis and oxidative stress are regarded as two indispensable contributors in ADR-induced myocardial injury [2]. Previous study demonstrated that ADR could directly induce apoptosis [3]. And it also has been reported that excessive reactive oxygen species (ROS) production induced by ADR in the heart could disrupt cellular membrane

Abbreviations: ADR, adriamycin; AMPK, AMP-activated protein kinase; *Anp*, atrial natriuretic peptide; *Bnp*, brain natriuretic peptide; *Cat*, catalase; *Ctgf*, connective tissue growth factor; DOX, doxorubicin; FGF1, fibroblast growth factor 1; FGFR, fibroblast growth factor receptor; *Gsta3*, glutathione s-transferase a3; *Ho-1*, heme oxygenase-1; *Il6*, interleukin 6; MDM2, murine double minute 2; *Myh7*, β-myosin heavy chain; *Nqo1*, NAD(P)H quinone oxidoreductase 1; Nrf2, nuclear factor erythroid 2-related factor 2; ROS, reactive oxygen species; *Sod*, superoxide dismutase; *Tgfb1*, transforming growth factor β1; *Tnfa*, tumor necrosis factor-α; 4-HNE, 4-Hydroxynonenal.

* Corresponding author. School of Nursing and Rehabilitaion, Cheeloo College of Medicine, Shandong University, Address: No. 44, Wenhua West Road, Jinan, Shandong, 250012, China.
E-mail address: junlian_gu@sdu.edu.cn (J. Gu).

https://doi.org/10.1016/j.redox.2021.102219
Received 24 October 2021; Received in revised form 5 December 2021; Accepted 17 December 2021
Available online 18 December 2021

integrity and aggravate cardiomyocyte apoptosis [3,4]. Therefore, Cardiac therapy designed to attenuate cell apoptosis and oxidative stress are promising strategies to slow the occurrence and progression of ADR-induced cardiotoxicity.

Fibroblast growth factor 1 (FGF1) is also called acidic FGF (aFGF), and belongs to the FGFs family. FGF1 acts as an effective endogenous mitogen by binding to heparin and FGF receptor (FGFR) *in vivo* [5,6]. Recently, FGF1 displays great abilities on maintaining glucose and lipid metabolic homeostasis [7,8]. Furthermore, it has been proved that wild-type FGF1 ($FGF1^{WT}$) possesses anti-oxidative stress [9] and anti-apoptosis [10] activity in the treatment of various diseases. In addition, $FGF1^{WT}$ also shows favorable effects on improving cardiac diseases such as ischemia/reperfusion injury [11], myocardial infarction [12], and diabetic cardiomyopathy [13]. Therefore, $FGF1^{WT}$ may have potency on the prevention and treatment of ADR-induced cardiotoxicity. However, chronic application of $FGF1^{WT}$ could raise the risk of tumorigenesis due to its powerful proliferative effects [14]. Hence, a FGF1 variant called $FGF1^{\Delta HBS}$ has been engineered, and $FGF1^{\Delta HBS}$ shows reduced ability to result in heparan sulfate (HS)-dependent FGF-FGFR binding and dimerization in our and other previous studies [15,16]. As expected, $FGF1^{\Delta HBS}$ exhibits much lower mitogenic potential, and keeps full metabolic activities *in vitro* and *in vivo* compare to $FGF1^{WT}$ [15]. We and others demonstrated that $FGF1^{\Delta HBS}$ could alleviate multiple of organ injury by improving lipid metabolism and suppressing oxidative stress and inflammation [15–17]. Despite these promising results, the potential mechanisms have not been clearly identified. Furthermore, the activity of $FGF1^{\Delta HBS}$ to protect against pathophysiological and morphological alterations in the heart has not been tested in ADR-based chemotherapy.

To answer the above questions, we therefore established ADR-induced cardiotoxicity in a mouse model, as described previously [2], and treated with and without $FGF1^{\Delta HBS}$ for 1 month. Functional, pathological and biochemical changes of the heart were examined at the 1 month of $FGF1^{\Delta HBS}$ treatment. To mechanistically study, transgenic mice with a cardiac deletion of sirtuin 1(*Sirt1*-CKO) gene were used in combination of cultured cardiac cells *in vitro* with p53-specific stabilizer (nutlin-3a) were introduced to identify the role and underlying mechanism of $FGF1^{\Delta HBS}$ in reducing cardiotoxicity caused by ADR.

2. Materials and methods

2.1. Animals and treatments

C57BL/6J male mice were purchased from Vital River Laboratories (Beijing, China). Mice were allowed tap water and rodent chow, and were maintained at 22 °C with a 12h light-12h dark cycle. All mice were acclimatized for 1 week before experimentation. For animal study, mice were randomly divided into four groups (6 mice per group): Control, $FGF1^{\Delta HBS}$, ADR, and ADR + $FGF1^{\Delta HBS}$. Mice were pretreated with $FGF1^{\Delta HBS}$ (0.5 mg/kg, a gift from School of Pharmaceutical Sciences at the Wenzhou Medical University) or vehicle (0.9% saline) via intraperitoneal injection every other day based on our previous study [15], a week later, followed with or without intraperitoneal injection of ADR (5 mg/kg, MedChemExpress, Monmouth Junction, NJ, USA) one day of each week for 3 weeks. At the end of the ADR plus $FGF1^{\Delta HBS}$ treatment, cardiac function of mice was examined by echocardiography, then mice hearts were obtained for the measurement of expression of mRNA, protein, and histopathological analyses. All animal protocols and experiments were approved by the Animal Care and Utilization Committee of Shandong University (Shandong, China).

Cardiac specific knockout of *Sirt1* (*Sirt1*-CKO) mice in a C57BL/6J background were generated by crossing $Sirt1^{flox/flox}$ mice with Myh6-CreEsr1 mice, and *Sirt1*-CKO mice were injected with tamoxifen 40 mg/kg/day for 3 consecutive days and rested for 1 week before next experimentation.

2.2. Cell culture and treatments

Primary cardiomyocytes were harvested from neonatal Sprague Dawley rat hearts, briefly, the hearts of rats (0.5–3 days) were isolated and treated with collagenase (Sigma-Aldrich, St. Louis, MO, USA) for dissociation. The cells were plated in 100-mm culture dishes in low-glucose Dulbecco's modified Eagle's medium (DMEM, Macgene, Beijing, China) with 10% new-born calf serum, 6% horse serum (Kang Yuan biology, Zibo, China), 1% 5-Bromo-2′-deoxyuridine (Sigma-Aldrich), 100U/ml penicillin and 100 μg/ml streptomycin (Gibco, Grand Island, NY, USA) for 1.5 h. Then, suspended cells were harvested as cardiomyocytes, plated in six-well plates for next studies. Embryonic rat myocardium-derived cells (H9c2) cells were cultured in high-glucose DMEM (Macgene, Beijing, China) supplemented with 10% fetal bovine serum (Gibco), 100U/ml penicillin and 100 μg/ml streptomycin. Primary cardiomyocytes and H9c2 cells were maintained in a 37 °C humidified incubator of 5% CO_2. For the mechanistic study, cells were pretreated with phosphate buffered saline (PBS) or $FGF1^{\Delta HBS}$ for 2 h when 80% confluency was reached [2,16], followed by 1 μM ADR for 24h at 37 °C. When the treatment is completed, cells was prepared for biochemical analysis. To ensure the effective concentration of $FGF1^{\Delta HBS}$, 100, 250 and 500 ng/ml $FGF1^{\Delta HBS}$ were added to cells. To stabilize p53, 10 μM nutlin-3a (APExBIO Technology LLC, Houston, TX, USA) [18] was added with 100 ng/ml $FGF1^{\Delta HBS}$. For the study on the down-regulation of *Sirt1 and* nuclear factor erythroid 2-related factor 2 (*Nrf2*) gene expression, bacterial stab of the plasmid short hairpin RNA-negative control (NC-shRNA), *Sirt1*-shRNA and *Nrf2*-shRNA were purchased from GenePharma (Shanghai, China). According to the manufacturer's instructions, purified plasmid DNA by Lipofectamine 3000 (Invitrogen, Grand Island, NY, USA) was transfected to cells at 70%–90% confluence. To measure the half-life of p53, 10 μM cycloheximide (CHX) was added after cells were treated with PBS or 100 ng/ml $FGF1^{\Delta HBS}$ for 24h.

2.3. Echocardiography

Cardiac function was determined in anesthetized mice. Briefly, mice were sedated with isoflurane (RWD Life Science inc. Shenzhen, China), then mice were placed on a heating pad in a supine position. Monitoring the heart rate of mice (ranged from 400 to 550 beats per minute), then cardiac function was measured using a Vevo 2100 High-Resolution Imaging System (Visual Sonics, Toronto, ON, Canada) with a ultrasonic LZ 400 probe (automatic focus, frequency 40.0 MHz) as previously described [19]. Echocardiography analysis mainly include the parameters of left ventricle (LV) internal dimension (LVID), LV posterior wall thickness (LVPW), interventricular septum thickness (IVS), LV mass, ejection fraction (EF), and fractional shortening (FS).

2.4. Quantitative real-time PCR

TRIzol reagent (Cwbio, Valencia, CA, USA) was used for total RNA extraction. A HiFiScript cDNA Synthesis Kit (Cwbio) was used for the reverse transcription of RNA. mRNA levels of related genes were tested as described previously [20]. The primers targeting *Fgf1*, β-myosin heavy chain (*Myh7*), atrial natriuretic peptide (*Anp*), brain natriuretic peptide (*Bnp*), connective tissue growth factor (*Ctgf*), transforming growth factor β (*Tgfb*), tumor necrosis factor-α (*Tnfa)*, interleukin 6 (*Il6*), catalase (*Cat*), superoxide dismutase (*Sod*), heme oxygenase-1 (*Ho-1*) and NAD(P)H quinone oxidoreductase 1 (*Nqo1*) were purchased from Sangon Biotech (Shanghai, China). Fold differences between mRNA abundance were determined using comparative cycle time (Ct) and β-actin (*Actb*) was served as standard.

2.5. Western blot analysis

Target protein quantification was performed by using Western blot. Briefly, the heart tissues or harvested cells were homogenized in RIPA

lysis buffer (Beyotime Biotechnology, Shanghai, China), the liquid supernatant was obtained by centrifugation at 12000 rpm for 25 min at 4 °C for Western blot analysis. The proteins were separated on 10% polyacrylamide gels using SDS-PAGE and transferred to nitrocellulose membranes (GE Healthcare Life Sciences, Beijing, China). Membranes were blocked in 5% non-fat milk, and these membranes were incubated at 4 °C overnight with the antibodies from Cell Signaling Technology: anti-cleaved caspase-3, anti-Sirt1, anti-p-AMP-activated protein kinase (AMPK), anti-total AMPK (anti-T-AMPK), and anti-Acetyl-p53 (Ac-p53) at a dilution of 1:1000. Other primary antibodies including anti-FGF1, anti-Nrf2, anti-4-Hydroxynonenal (4-HNE), (1:1000 dilution, Abcam, Cambridge, USA), anti-p53, anti-murine double minute 2 (MDM2), Sirt6, Sirt7 (1:1000 dilution, Proteintech, Chicago, IL, USA), as well as Glyceraldehyde 3-phosphate dehydrogenase (GAPDH) (1:1000 dilution, Servicebio technology, Wuhan, China). After incubated with the horseradish peroxidase (HRP)-conjugated secondary antibody (1:1000, Proteintech) at room temperature for 1.5 h, the signal intensities were visualized by an enhanced chemoluminescence detection kit (Millipore, Billerica, MA, USA), and analyzed using Image Quant 4.2 software (Tanon, Shanghai, China).

2.6. Histology and various staining

The heart tissues fixed in 10% buffered formalin were dehydrated and cleared through graded alcohol series and xylene, embedded in paraffin, and cut into 5 μm sections. Hematoxylin & eosin (H&E) staining was used for observing cardiac histological morphology. Fluorescein isothiocyanate-conjugated wheat germ agglutinin (FITC-conjugated WGA, Sigma-Aldrich) for the cross-sectional histological analysis of myocyte. Masson's trichrome and Sirius-red staining for collagen accumulation by using a Masson stain kit (Servicebio) and a Sirius red stain kit (Leagene Biotechnology, Beijing, China).

For immunohistochemical (IHC) staining, heart sections were incubated with primary antibodies: TNF-α, Nrf2 and 4-HNE (1:200 dilution, Abcam) as described previously [19,21]. After incubated in HRP-conjugated secondary antibodies, sections were incubated in peroxidase substrate 3,3-Diaminobenzidine (DAB, Servicebio technology) and counter stained with hematoxylin. All the sections were observed by biological microscope (Nikon, Tokyo, Japan) and quantified by Image J software.

For fluorescence staining, frozen myocardial tissues were fixed by 4% paraformaldehyde for 20 min. ROS production was evaluated by dihydroethidium (DHE) fluorescence Kit obtained from Beyotime Biotechnology (Shanghai, China). To evaluate myocardial apoptosis, sections of heart tissues were stained by using Terminal deoxynucleotidyl transferase dUTP nick-end labeling (TUNEL) apoptosis detection kit (Keygen Biotech) or In Situ Cell Death Detection Kit from Sigma-Aldrich and counter stained with DAPI (Abcam). H9c2 cells were incubated with 2′,7′-Dichlorofluorescin diacetate (DCFH-DA, Beyotime Biotechnology) probes for 20 min to detect ROS levels. Stained sections and H9c2 cells were evaluated by a fluorescence microscope (Nikon, Tokyo, Japan).

2.7. Flow cytometry

Cell apoptosis was detected by an Annexin V-FITC/propidium iodide (PI) kit (BD Bioscience, NJ, USA). H9c2 Cells were first trypsinized and then washed twice by PBS. After adding the binding buffer, cells were incubated with 5 μl of Annexin V-FITC and 5 μl of PI in the darkness for 15 min, then cell were analyzed with Cyto FLEX S (Beckman, USA) [22]. ROS production was evaluated by flow cytometry of DCF *in vitro* [2]. Briefly, The H9c2 cells were stained with DCFH-DA after exposed to their corresponding treatment at 37 °C for 30 min in a darkroom. Flow cytometry was then used for analysis and the extent of oxidative stress was measured by the mean fluorescence intensity.

2.8. Immunoprecipitation

For p53 ubiquitination analysis, H9c2 cells were treated with 100 ng/ml FGF1$^{\Delta HBS}$ for 2h prior to addition of 1 μM ADR for 24 h and lysed by using IP lysis buffer (Beyotime) containing protease and phosphatase inhibitors; then the lysates were incubated with antibody anti-p53 and 40 μl protein A/G PLUS-agarose beads (Santa Cruz Biotechnology) at 4 °C overnight, the beads were harvested through centrifugation. The immunocomplexes were detected by Western blot with an anti-ubiquitin antibody (1:1000, Abcam).

2.9. Statistical analysis

Data are shown as means ± standard deviation (SD). Two-tailed *t*-test was used to compare two groups and One-way analysis of variance (ANOVA) followed by Turkey test or Bonferroni test was used to compare three or more groups, Two-way ANOVA followed by Turkey test was used to compare the effects of knockout or knockdown *of Sirt1* or *Nrf2* in response to FGF1$^{\Delta HBS}$ treatment. All statistical data were analyzed by using GraphPad Prism v8.0.2.263 data analysis and graphing software. $P < 0.05$ was considered statistically significant.

3. Results

3.1. Decreased FGF1 expression in mice heart tissues, primary cardiomyocytes and H9c2 cells treated with ADR

To explore whether there has possible correlation between ADR-induced cardiotoxicity and FGF1, we detected the expression of endogenous FGF1. Compared to Control group, the mRNA expression of *Fgf1* were decreased in ADR-treated mice heart tissues (Fig. 1A). Evident reduction in mRNA level of *Fgf1* was also observed in primary cardiomyocytes (Fig. 1B) and H9c2 cells (Fig. 1C) treated by ADR in a dose-dependent manner. Consistent with the data of *Fgf1* mRNA level, protein expression of FGF1 in ADR-treated mice heart tissues (Fig. 1D), primary cardiomyocytes (Fig. 1E) and H9c2 cells (Fig. 1F) treated by ADR were obvious decreased relative to the Control group, respectively.

3.2. FGF1$^{\Delta HBS}$ protected against ADR-induced cardiac pathological and functional abnormalities

To define whether FGF1$^{\Delta HBS}$ protects against ADR-induced cardiotoxicity, mice were given intraperitoneal injection of ADR (5 mg/kg, once a week for three times), and a treatment of FGF1$^{\Delta HBS}$ (0.5 mg/kg, every other day beginning one week prior to injection of ADR and lasting for 4 weeks). Cardiac dysfunction was reflected by obvious increased LV volume and decreased EF and FS in ADR group, whereas treatment with FGF1$^{\Delta HBS}$ significantly prevented cardiac dysfunction induced by ADR (Fig. 1G–I and other echocardiographic parameters in Table S1).

Hearts from ADR group presented apparent myofiber disarray, defined by H&E staining (Fig. 2A). Furthermore, hypertrophic cardiomyocytes in ADR group were evident by analysis of myocyte area via FITC-conjugated WGA staining (Fig. 2B&C). Morphological hypertrophy of the heart from ADR group was further confirmed by the progressively increased mRNA expression of the molecular hypertrophy markers *Myh7*, *Anp*, and *Bnp* (Fig. 2D–F). However, all these indices related to myofiber disarray and hypertrophy caused by ADR were inhibited by FGF1$^{\Delta HBS}$ treatment (Fig. 2A–F).

It has been proved that ADR-induced cardiac fibrosis and inflammation accelerate the development of cardiac dysfunction and remodeling [23,24]. Therefore, whether FGF1$^{\Delta HBS}$ protects against ADR-induced fibrosis and inflammation was examined. The cardiac fibrotic response, determined by increased collagen accumulation via Masson's trichrome staining (Fig. 2G&I) and Sirius Red staining (Fig. 2H&J), and the mRNA expression of fibrotic mediators *Ctgf* (Fig. 2K) and *Tgfb* (Fig. 2L), all these indices were evident in the ADR

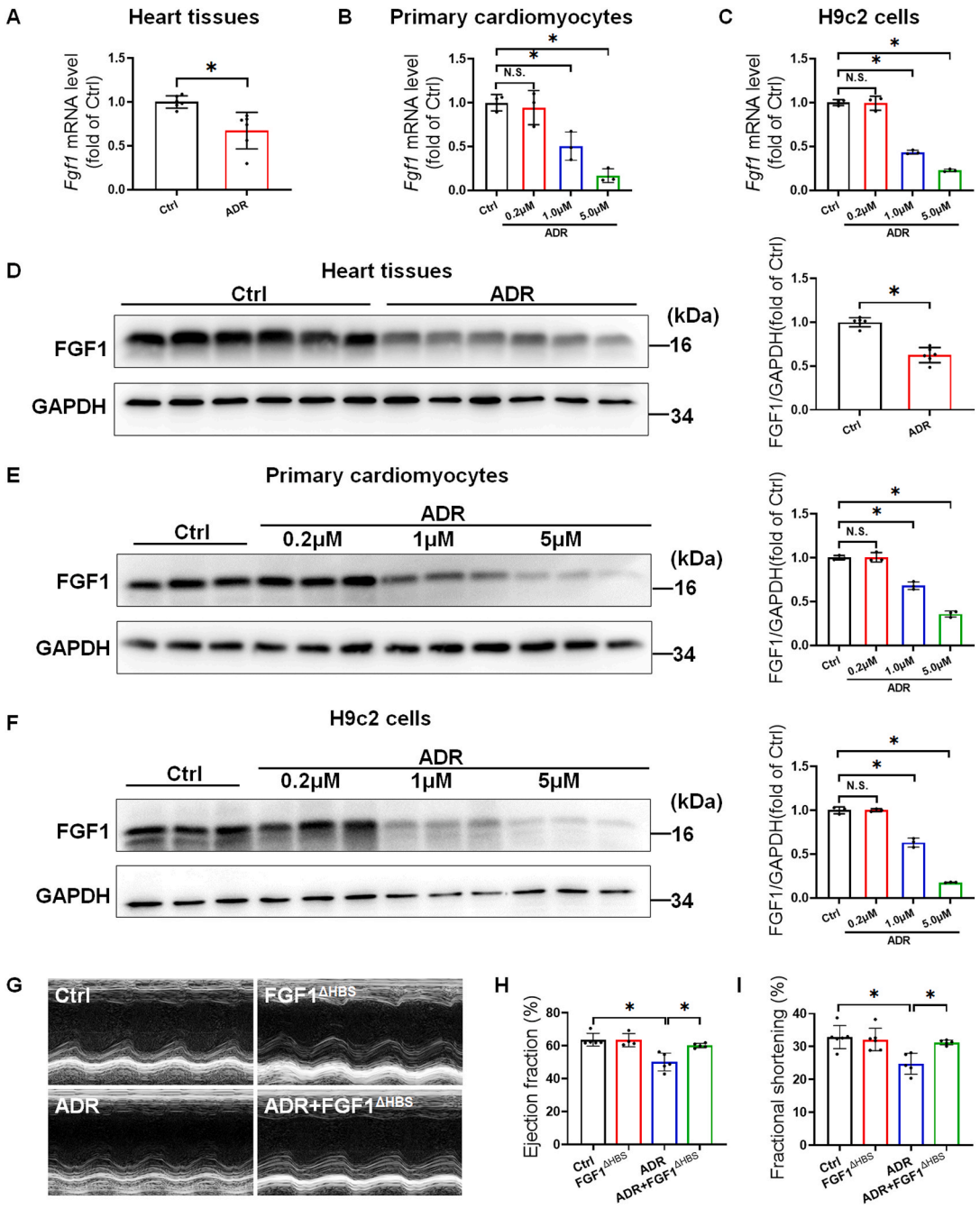

Fig. 1. Decreased endogenous FGF1 levels in ADR-treated cardiomyocytes and FGF1$^{\Delta HBS}$ alleviated ADR-induced cardiac dysfunction. A) The mRNA expression of *Fgf1* in heart tissues (n = 6). B) The mRNA expression of *Fgf1* in primary cardiomyocytes. C) The mRNA expression of *Fgf1* in H9c2 cells. D) The protein expression of FGF1 in heart tissues was analyzed by Western blot and quantification of the relative protein levels (n = 6). E) The protein expression of FGF1 in primary cardiomyocytes was analyzed by Western blot and quantification of the relative protein levels. F) The protein expression of FGF1 in H9c2 cells was analyzed by Western blot and quantification of the relative protein levels. G-I) Cardiac function was examined by echocardiography. G) Representative M-mode echocardiograms. H) Ejection fraction (n = 4–5). I) fractional shortening (n = 5–6). GAPDH as an internal control. Three independent experiments were performed in primary cardiomyocytes and H9c2 cells. Data are presented as means ± SD. *$P < 0.05$; N.S., not significant. Ctrl: Control.

group. Moreover, increased expression of inflammatory cytokines TNF-α in ADR-treated heart was visibly detected by IHC staining (Fig. 2M&N). Also, *Tnfa* and *Il6* mRNA expression were evident in ADR group (Fig. 2O&P). Whereas, FGF1$^{\Delta HBS}$ treatment largely reduced cardiac inflammation and fibrosis induced by ADR (Fig. 2G-P).

3.3. *FGF1$^{\Delta HBS}$ protected against ADR-induced cardiac oxidative stress*

It has been reported that oxidative stress plays a vital role in ADR-induced cardiac damage [23]. Therefore, cardiomyocyte ROS level was defined by fluorescent probes DHE and DCFH-DA. ADR treatment significantly increased ROS level compare to Control group (Fig. 3A & Fig. 5A–B). In addition, levels of the lipid peroxidation marker protein 4-HNE, defined by IHC staining, were significantly increased in the ADR group (Fig. 3B). However, all these changes were obviously reduced by FGF1$^{\Delta HBS}$-treated ADR group (Fig. 3A–B & Fig. 5A–B).

Since Nrf2 is an antioxidant factor and play antioxidant role by promoting transcription of its downstream antioxidant genes such as

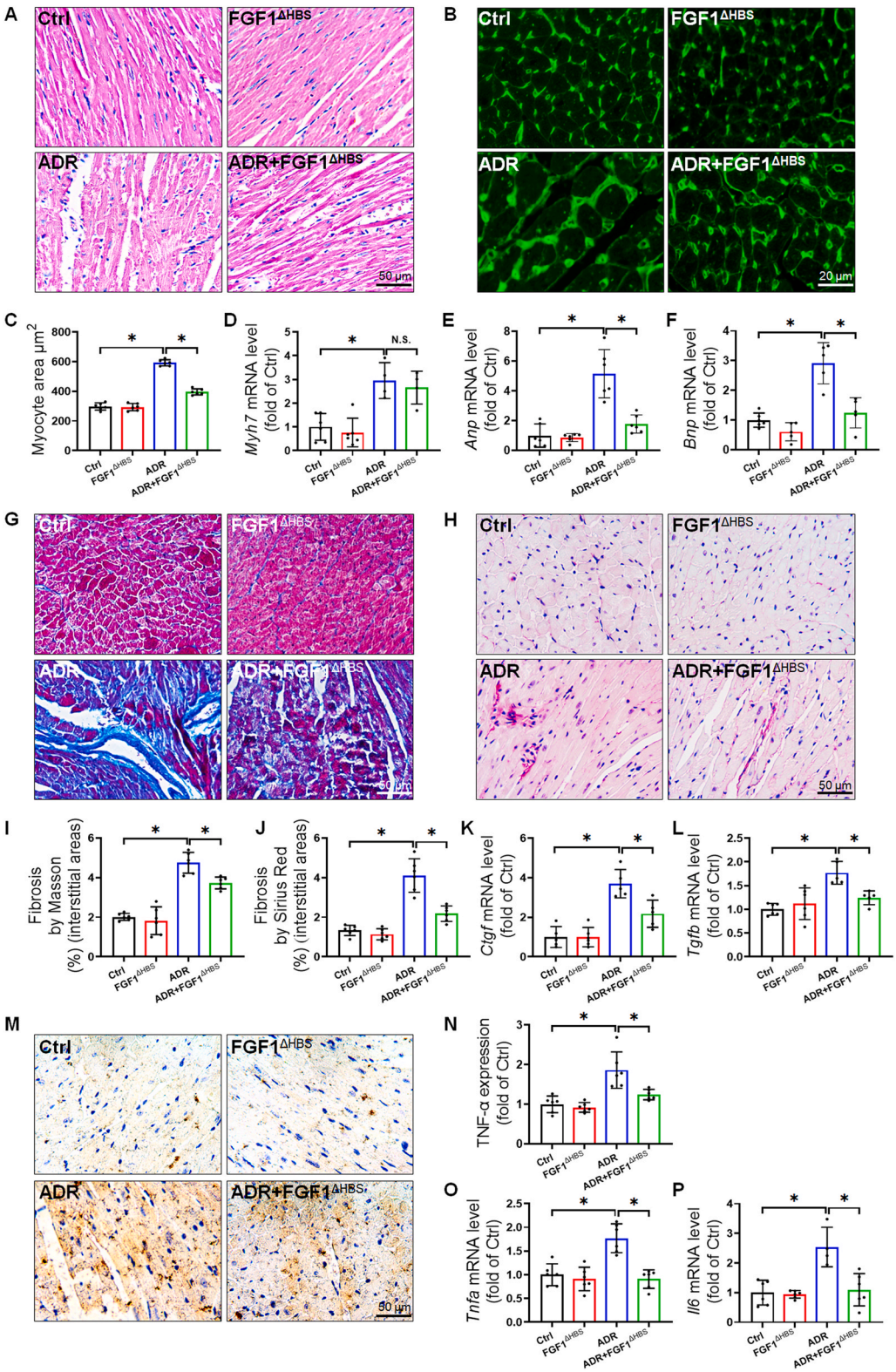

Fig. 2. FGF1$^{\Delta HBS}$ ameliorated ADR-induced cardiac pathological abnormalities. A) Cardiac histology, tested by H&E staining. B–C) Cardiac tissue FITC-conjugated WGA staining and quantification of myocytes cross-sectional areas (n = 6). D-F) The mRNA levels of hypertrophic markers β-myosin heavy chain (*Myh7*) (n = 4–6); atrial natriuretic peptide (*Anp*) (n = 6); brain natriuretic peptide (*Bnp*) in cardiac tissues (n = 5–6). G-J) Cardiac fibrotic response. G) determined by Masson's trichrome staining of collagen deposition (collagen is blue) and I) related quantitative analysis (n = 6). H) assessed by Sirius Red staining of collagen accumulation (collagen is red) and J) related quantitative analysis (n = 6). K) The mRNA expression of myocardial fibrosis markers connective tissue growth factor (*Ctgf*) (n = 5–6). L) transforming growth factor β (*Tgfb*) (n = 5–6) M − P) Cardiac inflammation damage. M) detected by IHC staining with tumor necrosis factor-α (TNF-α) (brown considered positive staining) and N) related quantitative analysis (n = 6). O) Relative mRNA levels of inflammatory markers *Tnfa* (n = 6) and P) interleukin 6 (*Il6*) (n = 4–6). Data are presented as means ± SD. *$P < 0.05$; N.S., not significant. (For interpretation of the references to colour in this figure legend, the reader is referred to the Web version of this article.)

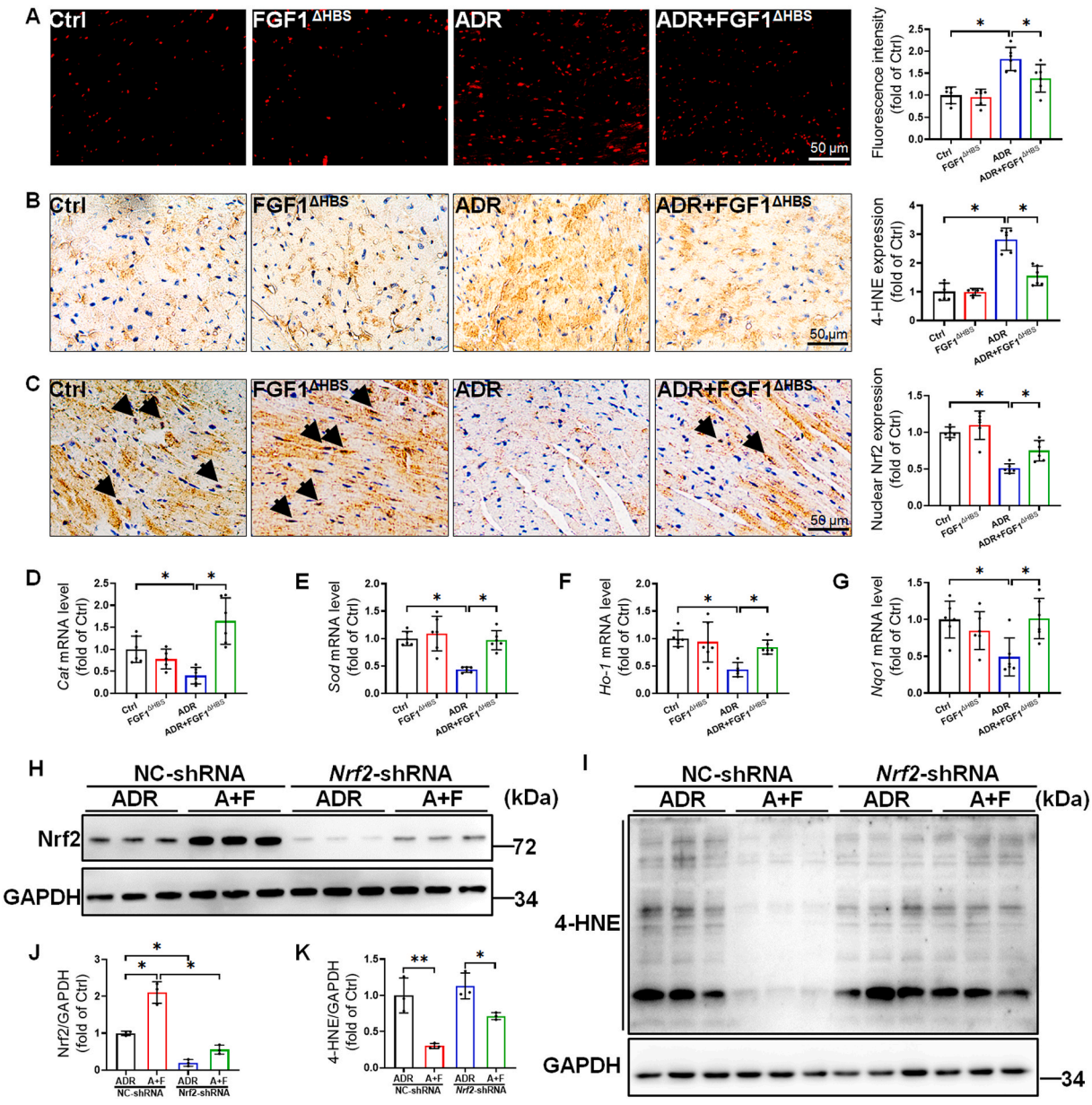

Fig. 3. FGF1$^{\Delta HBS}$ ameliorated ADR-induced oxidative stress A) Representative images of DHE staining in cardiac tissues followed by quantification of fluorescence intensity (n = 6). B) IHC staining using 4-Hydroxynonenal (4-HNE) antibody in cardiac tissues (brown considered positive staining) and related quantitative analysis (n = 6). C) Nuclear factor erythroid 2-related factor 2 (Nrf2) nucleus accumulation (indicated by black arrows) was detected by IHC staining with Nrf2 antibody (brown) and related quantitative analysis (n = 6). D-G) The mRNA levels of catalase (*Cat*) (n = 5–6); superoxide dismutase (*Sod*) (n = 6); heme oxygenase-1 (*Ho-1*), (n = 5–6); NAD(P)H quinone oxidoreductase 1 (*Nqo1*) in the cardiac tissues (n = 6). H–K) H9c2 cells were transfected with NC-shRNA or *Nrf2*-shRNA for 24h, then H9c2 cells were treated with PBS or 100 ng/ml FGF1$^{\Delta HBS}$ for 2 h, and subsequently treated with ADR (1 μM) for 24h. H) The Nrf2 and I) 4-HNE protein expressions were detected by Western blot and J-K) quantification of the relative protein levels. GAPDH as an internal control. Three independent experiments were performed in H9c2 cells. Data are presented as means ± SD. $^{*}P < 0.05$, $^{**}P < 0.001$. A + F: ADR + FGF1$^{\Delta HBS}$. (For interpretation of the references to colour in this figure legend, the reader is referred to the Web version of this article.)

Cat, *Sod*, *Ho-1* and *Nqo1* in multiple cardiac diseases, including cardiotoxicity induced by ADR [25]. We examined the expression of Nrf2 in cardiac tissues by IHC staining, the results showed that Nrf2 expression in the nuclei of cardiomyocytes is inhibited by ADR but significantly increased in the FGF1$^{\Delta HBS}$-treated ADR group (Fig. 3C). Then, the decreased expression of Nrf2 downstream antioxidant genes *Cat, Sod, Ho-1*, and *Nqo1* at mRNA levels further confirmed that Nrf2 transcriptional activity was inhibited in ADR group and significantly restored in FGF1$^{\Delta HBS}$-treated ADR group (Fig. 3D–G). To confirm the critical role of Nrf2 in the antioxidant effects of FGF1, knockdown of *Nrf2* gene was performed by *Nrf2*-shRNA. Nonsense shRNA did not alter Nrf2 expression and was used as control vector. Knockdown of *Nrf2* expression partly blocked the inhibitory effect of FGF1 on ADR-induced upregulation of 4-HNE (Fig. 3H–K), suggesting FGF1$^{\Delta HBS}$ protected against ADR-induced cardiac oxidative stress is partly mediated by Nrf2.

3.4. *FGF1$^{\Delta HBS}$ reduced ADR-induced cardiac injury by promoting the degradation of p53*

Cardiomyocyte apoptosis contributes to ADR-induced cardiac injury [24]. Therefore, whether FGF1$^{\Delta HBS}$ prevents ADR-induced cardiac apoptosis was examined. Numbers of TUNEL-positive cells were increased in the hearts of ADR group, and FGF1$^{\Delta HBS}$ significantly reduced cardiac TUNEL-positive cells caused by ADR (Fig. 4A).

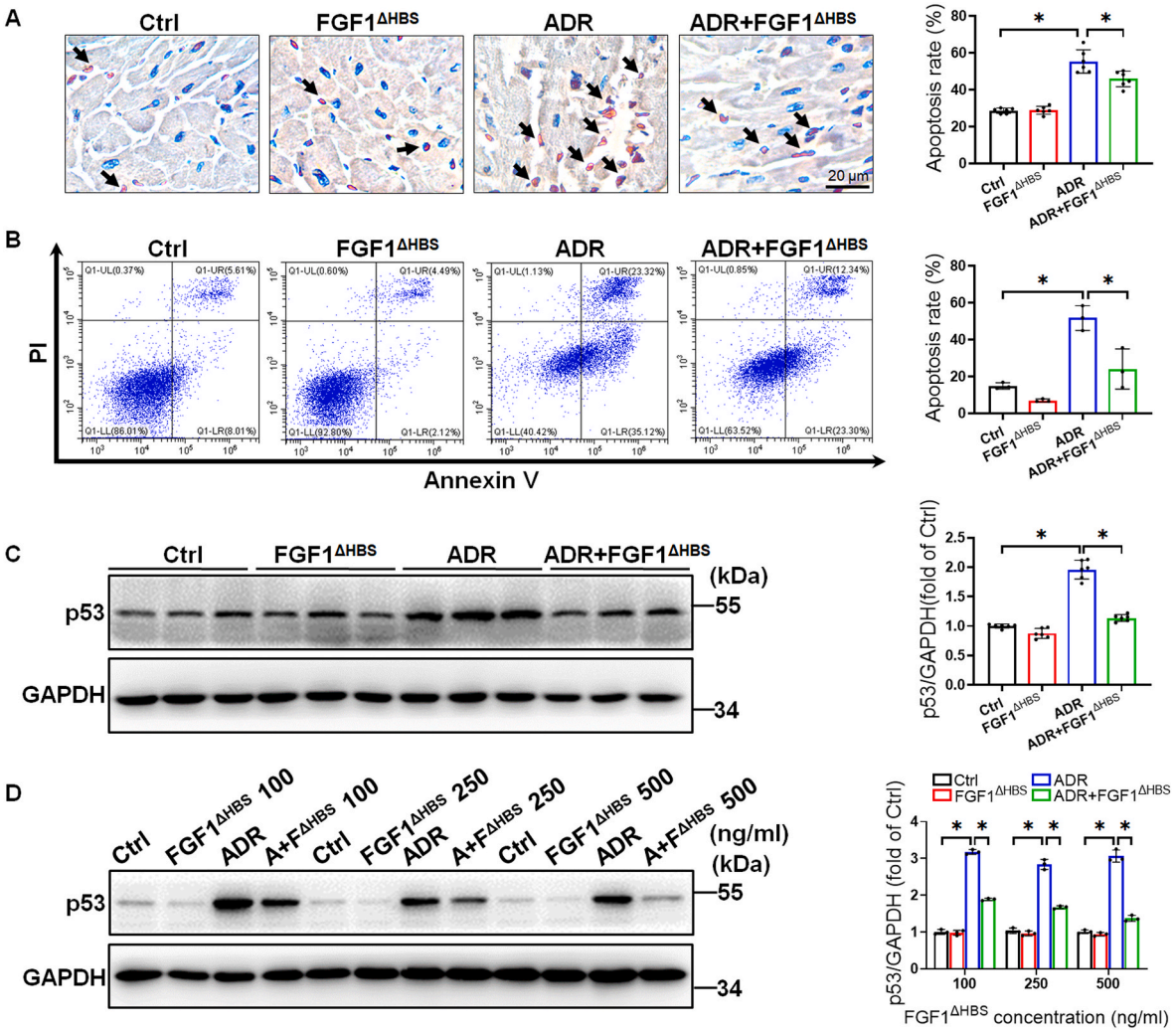

Fig. 4. FGF1$^{\Delta HBS}$ reduced ADR-induced cardiac apoptosis. A) Apoptotic cells (indicated by black arrows) was measured by TUNEL assay in mice heart tissues followed by quantification of apoptosis rate (n = 6). B) The apoptosis of H9c2 cells was detected by flow cytometry analysis using Annexin V-FITC/PI staining followed by related quantitative analysis. C) The protein expression of p53 in heart tissues was analyzed by Western blot and quantification of the relative protein levels (n = 6). D) H9c2 cells were treated with PBS or 100, 250, 500 ng/ml FGF1$^{\Delta HBS}$ for 2 h followed with or without addition of 1 μM ADR for 24 h and harvested for Western blot and quantification of the relative protein levels. GAPDH as an internal control. Three independent experiments were performed in H9c2 cells. Data are presented as means ± SD. *$P < 0.05$. A + F$^{\Delta HBS}$: ADR + FGF1$^{\Delta HBS}$.

Moreover, the apoptosis rate of H9c2 cells was detected by flow cytometry and the results were consistent with *in vivo* experiment (Fig. 4B).

In the past three decades, tumor suppressor protein p53 has received a great deal of research attention as an important intracellular pro-apoptotic factor. Multiple evidences have also shown a regulatory role for p53 both in the embryonic cardiac development and pathological cardiovascular diseases [26]. And the pathophysiological mechanism of ADR-induced cardiotoxicity appears to involve increased expression of p53 in cardiomyocytes, followed by severe cellular apoptosis [27]. Thus, we detected the protein expression of p53 in mice heart tissues and H9c2 cells by Western blot, both the *in vivo* and *in vitro* results showed that p53 expression was significantly increased in ADR-treated cardiomyocytes, and this effect was prevented by FGF1$^{\Delta HBS}$ (Fig. 4C&D). Of note, FGF1$^{\Delta HBS}$ suppressed p53 protein expression in a dose-dependent manner at ADR-treated H9c2 cells (Fig. 4D). In order to verify the role of p53 in the effects of FGF1$^{\Delta HBS}$ protects against ADR-induced cardiac injury. We up-regulated the expression of p53 in H9c2 cells by using nutlin-3a, a small-molecule activator of p53 by antagonizing the binding of MDM2 to p53 [18,28], thereby preventing MDM2-mediated p53 degradation, then we detected the ROS accumulation by fluorescent probes DCFH-DA (Fig. 5A&B), as well as cell apoptosis by both measuring the expression of cell apoptosis executor cleaved caspase-3 protein and detecting apoptotic positive cells by flow cytometry (Fig. 5C&D). The results showed that the up-regulation of p53 abolished the protection effects of FGF1$^{\Delta HBS}$ against ADR-induced cardiomyocyte ROS accumulation and apoptosis, which suggests FGF1$^{\Delta HBS}$ improved ADR-induced cardiac injury by inhibiting p53 protein expression.

To further explore potential mechanisms by which FGF1$^{\Delta HBS}$ treatment could lead to the inhibition of p53 protein expression, the half-life of p53 protein was examined in H9c2 cells with protein synthesis inhibitor CHX. In cells treated with PBS, the protein of p53 underwent decay at a half-life of 50 min, while this was shortened to 25 min in cells treated with FGF1$^{\Delta HBS}$ (Fig. 5E). These results indicated that FGF1$^{\Delta HBS}$ alleviate ADR-induced cardiac injury by promoting the degradation of p53.

3.5. FGF1$^{\Delta HBS}$ degraded p53 by MDM2-mediated p53 ubiquitination

MDM2, a p53-specific E3 ubiquitin ligase, is the principal cellular antagonist of p53, acting to promote p53 degradation by ubiquitinating p53 in unstressed cells [29,30]. Therefore, we explored whether

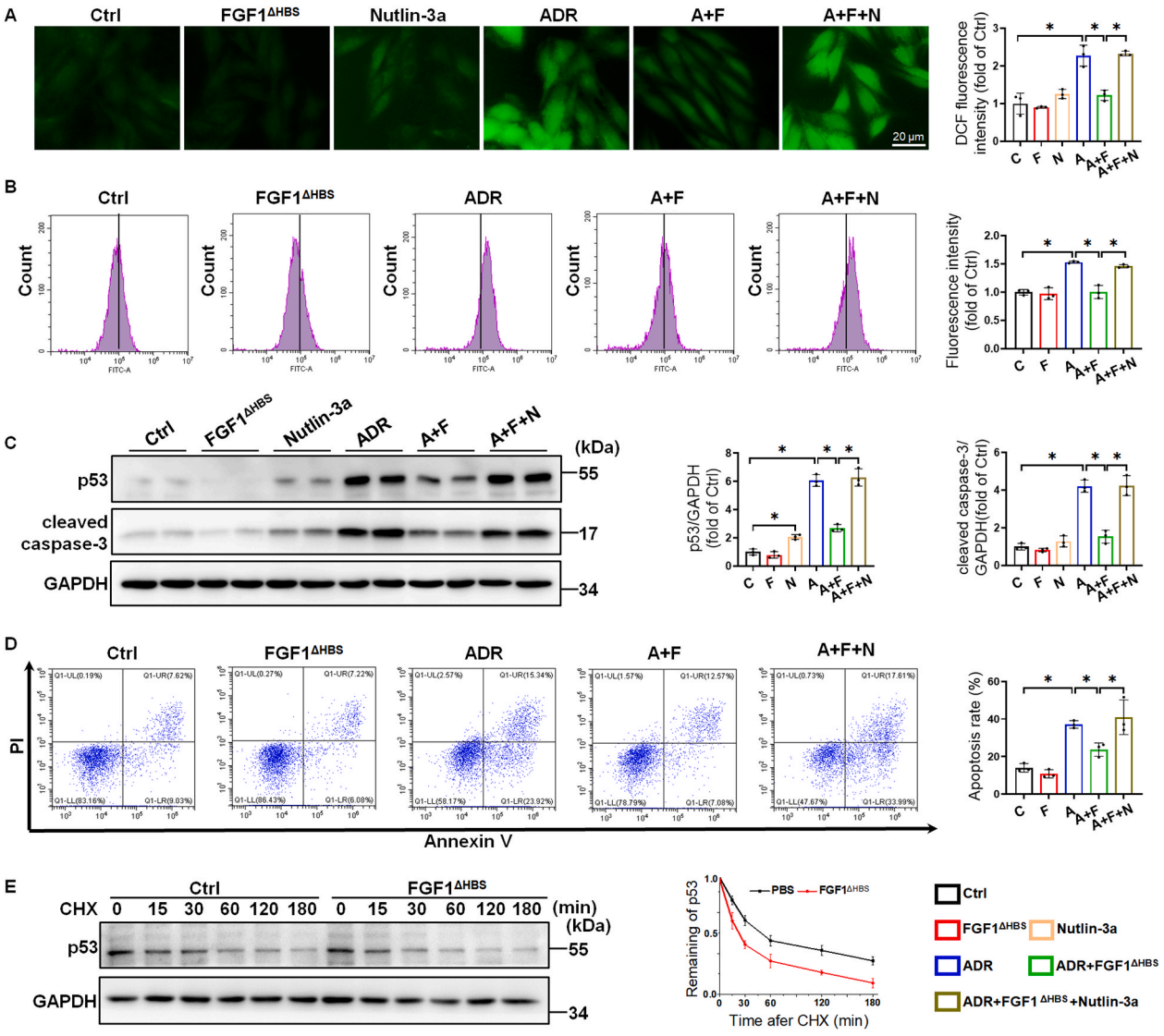

Fig. 5. FGF1$^{\Delta HBS}$ reduced ADR-induced cardiac injury by degrading p53. A-D) H9c2 cells were pretreated with PBS or 100 ng/ml FGF1$^{\Delta HBS}$ in the presence or absence of nutlin-3a (10 μM) for 2 h, and then treated with or without ADR (1 μM) for 24h. The ROS accumulation of H9c2 cell was analyzed by A) DCFH-DA staining and B) flow cytometry of DCF followed by quantification of fluorescence intensity. C) The p53 and cleaved caspase-3 protein expressions were detected by Western blot and quantification of the relative protein levels. D) H9c2 cells were stained using Annexin V-FITC/PI followed by related quantitative analysis. E) H9c2 cells were treated with PBS or 100 ng/ml FGF1$^{\Delta HBS}$ for 24h followed by 10 μM CHX treatment for indicated time and harvested for Western blot and quantification of the relative protein levels. GAPDH as an internal control. Three independent experiments were performed in H9c2 cells. Data are presented as means ± SD. *$P < 0.05$. C: Control; F: FGF1$^{\Delta HBS}$; N: Nutlin-3a; A: ADR; A + F: ADR + FGF1$^{\Delta HBS}$; A + F + N: ADR + FGF1$^{\Delta HBS}$ + Nutlin-3a.

FGF1$^{\Delta HBS}$ promote degradation of p53 is mediated by MDM2-induced p53 ubiquitination. The Western blot results in cardiac tissues, primary cardiomyocytes and H9c2 cells exhibited decreased protein expression of MDM2 in ADR group, while FGF1$^{\Delta HBS}$ elevated the expression of MDM2 inhibited by ADR (Fig. 6A for cardiac tissues, Fig. 6B for primary cardiomyocytes and Fig. S1 for H9c2 cells), To investigate whether the increased MDM2 expression was a reason of the degradation of p53 following FGF1$^{\Delta HBS}$ treatment. We detected if FGF1$^{\Delta HBS}$ promoted p53 degradation by a protein-protein interaction of ubiquitin with p53. Indeed, the interaction of ubiquitin and p53 was disturbed by ADR, which were corrected by FGF1$^{\Delta HBS}$-treated ADR group (Fig. 7A for primary cardiomyocytes and Fig. S2 for H9c2 cells). These finding indicated that FGF1$^{\Delta HBS}$ degraded p53 by increasing MDM2-mediated p53 ubiquitination.

3.6. *FGF1$^{\Delta HBS}$ promoted p53 ubiquitination by Sirt1-mediated p53 deacetylation*

The NAD$^+$ -dependent protein lysine deacylases of the sirtuin family regulate diverse physiological functions, from stress responses to energy metabolism. The human sirtuin isoforms, Srit1, Srit6 and Srit7, have been regarded as attractive therapeutic targets for heart-related diseases [31]. Studies also demonstrated that Srit1, Srit6 and Srit7 can inactivate p53 by promoting its deacetylation [32–35] and then facilitating p53 degradation [36]. To explore the role of Srit1, Srit6 and Srit7 in deacetylating p53 in our model, the expression of Sirt1, Sirt6 and Sirt7 protein was analyzed by Western blot in mice heart tissues, primary cardiomyocytes and H9c2 cells. The results showed that only Sirt1 expression was significantly down-regulated by ADR, which were

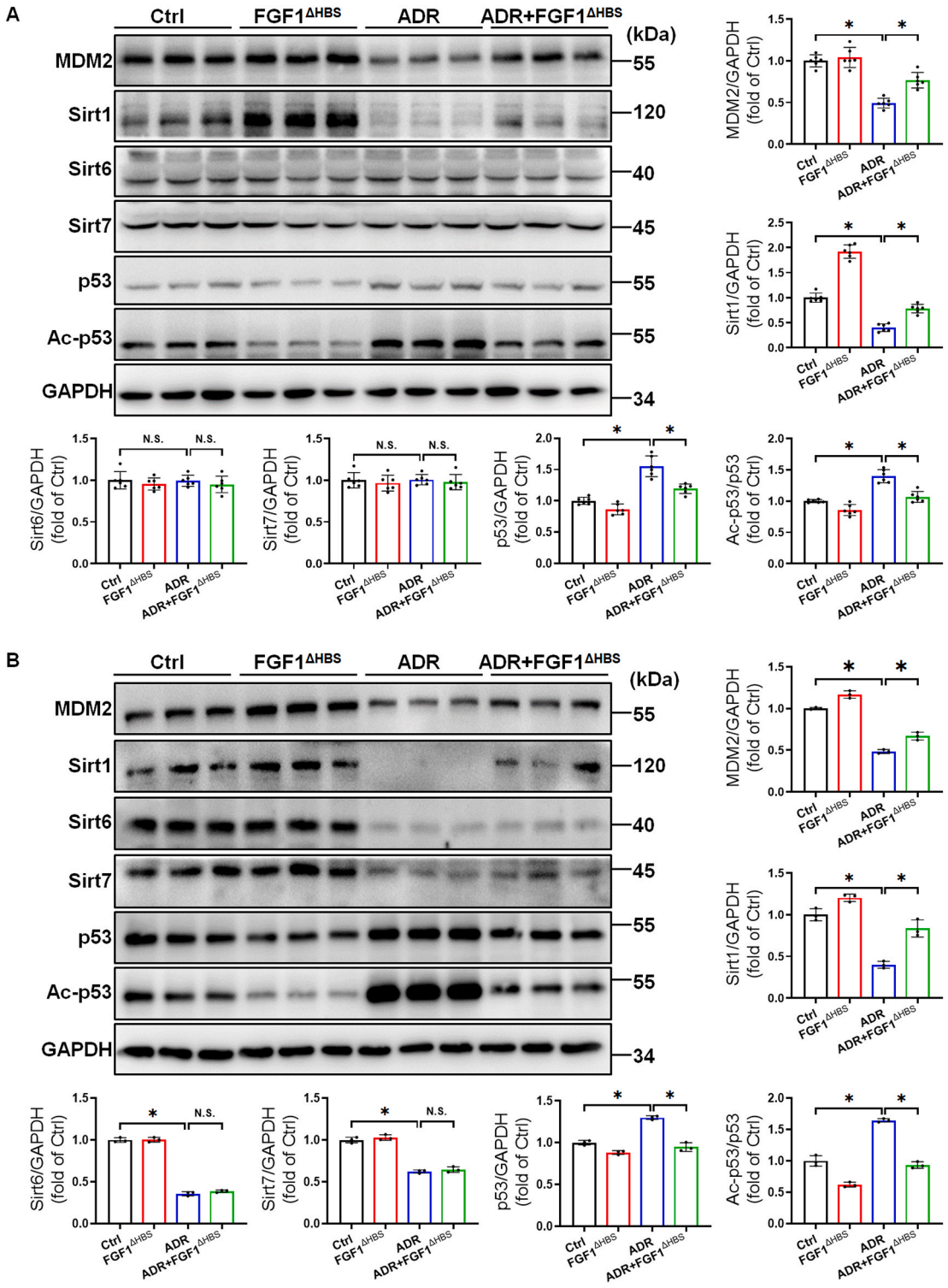

Fig. 6. FGF1$^{\Delta HBS}$ reversed ADR-disturbed the protein expression of MDM2, Sirt1 and Ac-p53 in cardiomyocytes. A) The related protein expressions were detected by Western blot in heart tissues and quantification of the relative protein levels (n = 6). B) Primary cardiomyocytes were treated with PBS or 100 ng/ml FGF1$^{\Delta HBS}$ for 2 h followed with or without 1 μM ADR for 24 h. The related protein expression were detected by Western blot and quantification of the relative protein levels, GAPDH as an internal control. Three independent experiments were performed in primary cardiomyocytes. Data are presented as means ± SD. *$P < 0.05$; N.S., not significant.

largely restored by FGF1$^{\Delta HBS}$ treatment in the ADR-treated mice and cells (Fig. 6A&B and Fig. S1). In addition, the Sirt6 and Sirt7 expression was not increased in FGF1$^{\Delta HBS}$/ADR group compare to ADR group (Fig. 6A&B and Fig. S1).

To determine whether the increase of Sirt1 promote the deacetylation of p53, the protein expression of Ac-p53 were analyzed by Western blot *in vivo* and *in vitro*. These results showed FGF1$^{\Delta HBS}$ reduced the increased expression of Ac-p53 induced by ADR (Fig. 6A&B and Fig. S1). Then, we down-regulated the expression of Sirt1 in H9c2 cells with *Sirt1*-shRNA, the results of Western blot indicated the knockdown

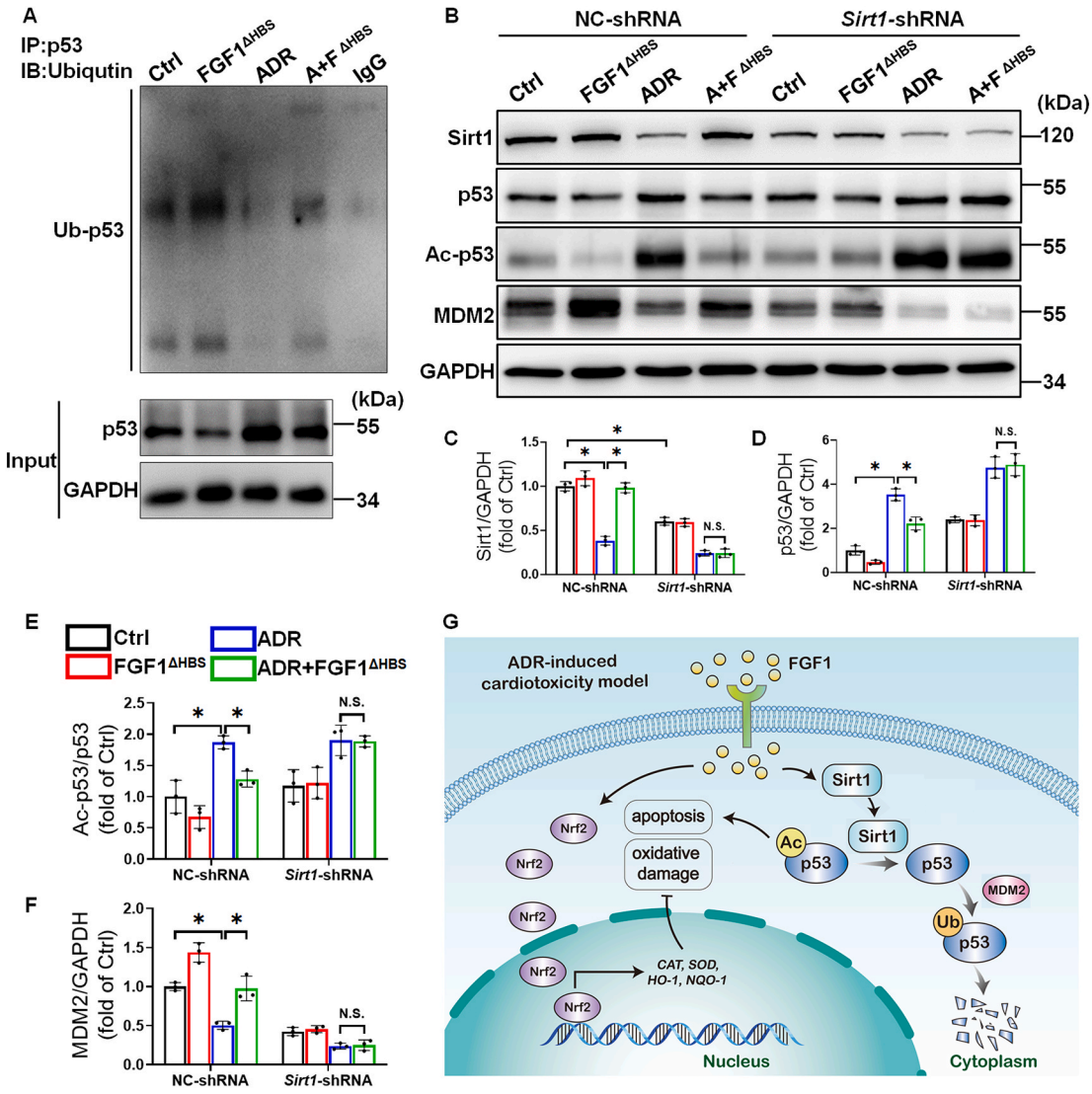

Fig. 7. The effect of FGF1$^{\Delta HBS}$ on MDM2-induced p53 ubiquitination is mediated by Sirt1. A) The immunoblotting of immunoprecipitated p53 with antibody recognized ubiquitin in primary cardiomyocytes. B) H9c2 cells were transfected with NC-shRNA or *Sirt1*-shRNA for 24h, then H9c2 cells were treated with PBS or 100 ng/ml FGF1$^{\Delta HBS}$ for 2 h, and subsequently treated with or without ADR (1 μM) for 24h. B–F) The protein expression of Sirt1, MDM2, Ac-p53, p53 were analyzed by Western blot followed by quantification of the relative protein levels. G) Schematic illustration for FGF1$^{\Delta HBS}$ protection against ADR-induced cardiotoxicity. Three independent experiments were performed in primary cardiomyocytes and H9c2 cells. GAPDH as an internal control. Data are presented as means ± SD. *$P < 0.05$; N. S., not significant. A + F$^{\Delta HBS}$: ADR + FGF1$^{\Delta HBS}$.

of *Sirt1* largely blocked the effect of FGF1$^{\Delta HBS}$ on decreasing p53 and Ac-p53, as well as the effect of FGF1$^{\Delta HBS}$ on increasing MDM2 in ADR group (Fig. 7B–F), suggesting Sirt1 contributed to the inhibitory effects of FGF1$^{\Delta HBS}$ on p53 by increasing the deacetylation of p53. Since acetylation and ubiquitylation of p53 occur on a similar set of lysine residues and are mutually exclusive [37], thus deacetylated p53 greatly accelerated the ubiquitination of p53 and the degradation of proteasome by MDM2.

3.7. Sirt1 mediated the protective effect of FGF1$^{\Delta HBS}$ against ADR-induced cardiotoxicity in vivo

To further confirm whether Sirt1 activation mediated the protective effects of FGF1$^{\Delta HBS}$ against ADR-induced cardiotoxicity, wild type (WT) and *Sirt1*-CKO mice were subjected to the ADR-induced cardiotoxicity model established by ADR injection. As expected, FGF1$^{\Delta HBS}$ treatment improved cell apoptosis (Fig. 8A) and cardiac oxidative stress (Fig. 8B&D) induced by ADR in WT mice but not in *Sirt1*-CKO mice, Similarly, FGF1$^{\Delta HBS}$ treatment improved the cardiac hypertrophy (Fig. 8C&E) and cardiac dysfunction (Table 1) in WT mice but not in *Sirt1*-CKO mice. Moreover, decreased Ac-p53 and increased MDM2 levels were observed in the heart of ADR-treated mice, which were normalized with FGF1$^{\Delta HBS}$ treatment in the ADR-treated WT mice but not in *Sirt1*-CKO mice (Fig. 8F–J). Taken together, these data indicate that Sirt1-mediated the protective effects of FGF1$^{\Delta HBS}$ on ADR-induced cardiotoxicity.

4. Discussion

Our previous studies have shown that FGF1$^{\Delta HBS}$ effectively ameliorated liver steatosis with reduced proliferation activity [15], however, there was no information for the effect and related mechanism of FGF1$^{\Delta HBS}$ on ADR-impaired pathological and functional alterations in the heart. In the current study, we revealed that mRNA and protein level of FGF1 was decreased in both ADR-treated mouse model and myocardial cell. These findings suggested the potential effect of FGF1 to protect against ADR-induced cardiotoxicity. Then, we identified FGF1$^{\Delta HBS}$ as a novel agent that possesses an ability to alleviate apoptosis and oxidative

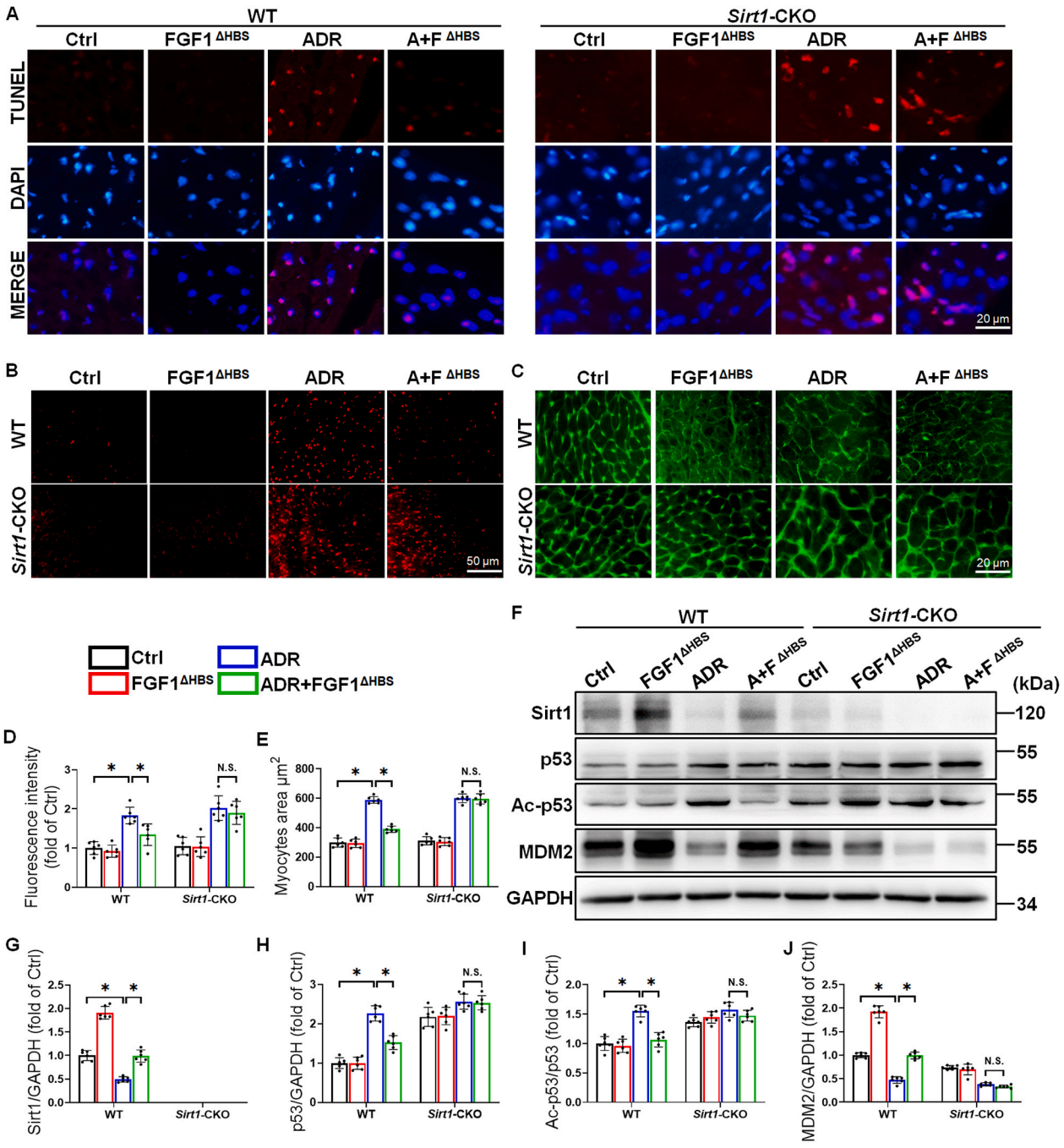

Fig. 8. *Sirt1*-CKO mice reduced FGF1$^{\Delta HBS}$ mediated cardiac protection and reversed the effect of FGF1$^{\Delta HBS}$ on the expression of MDM2 and Ac-p53. A) Representative images of TUNEL staining. B) Cardiac tissues were stained by DHE (Red) followed by D) quantification of fluorescence intensity (n = 6). C) Cardiac tissue FITC-conjugated WGA staining and E) quantification of myocytes cross-sectional areas (n = 6). F-J) The expression of Sirt1, MDM2, Ac-p53, p53 in cardiac tissues were analyzed by Western blot followed by quantification of the relative protein levels (n = 6). GAPDH as an internal control. Data are presented as means ± SD. *$P < 0.05$; N.S., not significant. (For interpretation of the references to colour in this figure legend, the reader is referred to the Web version of this article.)

stress of cardiomyocytes induced by ADR, significantly prevented cardiac remodeling and dysfunction. Further mechanism studies revealed that FGF1$^{\Delta HBS}$ prohibited p53 stability by Sirt1-mediated p53 deacetylation, then promoting MDM2-mediated p53 ubiquitination and proteasomal-dependent degradation.

The progression of ADR-induced cardiotoxicity is closely associated with increased oxidative stress in cardiomyocytes. Accumulating evidence demonstrates that excessive ROS production is detected in the heart and leads to mitochondrial dysfunction, subsequently affects the energy metabolism and results in death of cardiomyocytes after ADR treatment [25,38]. Therefore, antioxidative protection would be of great significance for treating ADR-related cardiotoxicity. Nrf2 is a key redox sensor and one of the main regulators of antioxidant response. Nrf2 could bind to regulatory antioxidant response elements and activate transcription of lots of antioxidant genes, such as *Nqo1*, glutathione s-transferase a3 (*Gsta3*), and *Ho*-1 that counteract ROS production [39]. Previous studies showed that nuclear Nrf2 activity was down-regulated in ADR-induced cardiotoxicity [25,40]. Furthermore, ADR-induced myocardial oxidative damage was further worsened by down-regulating Nrf2 expression [4]. Data from present study shown that expression of Nrf2 in the nucleus and its downstream antioxidant factors including *Cat*, *Sod*, *Ho-1* and *Nqo1* were decreased, accompanied with

Table 1
Protective effect of FGF1$^{\Delta HBS}$ on ADR-induced cardiac dysfunction in *Sirt1*-CKO mice.

	Ctrl	FGF1$^{\Delta HBS}$	ADR	FGF1$^{\Delta HBS}$/ADR
WT mice				
IVS,d	1.03 ± 0.06	1.04 ± 0.01	0.89 ± 0.05*	0.93 ± 0.01
LVID,d	3.02 ± 0.07	3.03 ± 0.03	3.32 ± 0.02*	3.06 ± 0.04$^{\#}$
LVPW,d	1.04 ± 0.02	1.03 ± 0.02	0.96 ± 0.03	1.07 ± 0.08
IVS,s	1.23 ± 0.06	1.26 ± 0.04	1.09 ± 0.06	1.07 ± 0.07
LVID,s	1.66 ± 0.04	1.63 ± 0.01	2.25 ± 0.05*	1.84 ± 0.05$^{\#}$
LVPW,s	1.94 ± 0.04	1.99 ± 0.07	1.61 ± 0.04*	1.62 ± 0.01
EF%	77.78 ± 0.58	79.09 ± 0.48	61.73 ± 1.42*	72.03 ± 1.46$^{\#}$
FS%	44.99 ± 0.53	46.27 ± 0.50	32.25 ± 0.97*	39.90 ± 1.21$^{\#}$
LV mass	110.28 ± 9.81	110.70 ± 3.03	107.02 ± 5.33	106.46 ± 5.63
LV mass,Co	88.23 ± 7.85	88.56 ± 2.42	85.62 ± 4.27	85.17 ± 4.50
LV Vol,d	35.71 ± 1.87	36.00 ± 0.95	44.84 ± 0.77*	36.62 ± 1.34$^{\#}$
LV,Vol,s	7.94 ± 0.53	7.53 ± 0.10	17.17 ± 0.94*	10.26 ± 0.77$^{\#}$
Sirt1-CKO mice				
IVS,d	0.93 ± 0.04	0.95 ± 0.03	1.01 ± 0.04	1.02 ± 0.03
LVID,d	3.09 ± 0.03	3.04 ± 0.003	3.26 ± 0.01*	3.24 ± 0.01
LVPW,d	1.07 ± 0.03	1.06 ± 0.06	1.01 ± 0.06	0.99 ± 0.05
IVS,s	1.24 ± 0.02	1.31 ± 0.01	1.13 ± 0.05*	1.15 ± 0.04
LVID,s	1.73 ± 0.01	1.70 ± 0.03	2.30 ± 0.02*	2.27 ± 0.03
LVPW,s	1.74 ± 0.03	1.98 ± 0.01	1.64 ± 0.02*	1.61 ± 0.03
EF%	76.67 ± 0.55	76.84 ± 0.98	57.38 ± 0.79*	58.40 ± 1.16
FS%	44.01 ± 0.53	44.12 ± 0.93	29.23 ± 0.53*	29.88 ± 0.79
LV mass	108.17 ± 5.67	105.63 ± 6.26	117.62 ± 2.18	116.30 ± 4.61
LV mass,Co	86.53 ± 4.54	84.50 ± 5.01	94.10 ± 1.74	93.04 ± 3.69
LV Vol,d	37.64 ± 0.75	36.10 ± 0.09	42.72 ± 0.27*	42.07 ± 0.15
LV Vol,s	8.78 ± 0.15	8.36 ± 0.35	18.21 ± 0.32*	17.51 ± 0.51

Data are presented as means ± SD.
IVS,d, end-diastolic interventricular septum thickness; LVID,d, left ventricle (LV) internal-diastolic diameter; LVPW,d, end-diastolic LV posterior wall thickness; IVS,s, end-systolic interventricular septum thickness; LVID,s, LV internal-systolic diameter; LVPW,s, end-systolic LV posterior wall thickness; EF, ejection fraction; FS, shortening fraction; LV mass,Co, LV mass, Corrected; LV vol,d, LV end-diastolic volume; LV vol,s, LV end-systolic volume.
*$P < 0.05$ vs. respective Control group; $^{\#}P < 0.05$ vs. respective ADR group.

severe oxidative damage in mice treated by ADR. However, all these changes were significantly alleviated by FGF1$^{\Delta HBS}$ treatment, and knockdown of Nrf2 expression partly blocked the inhibitory effect of FGF1 on ADR-induced oxidative damage (Fig. 3). Therefore, these results indicated that FGF1$^{\Delta HBS}$ protected against ADR-induced cardiotoxicity by improving redox homeostasis and attenuating oxidative stress in heart.

Another novelty finding in this study is that FGF1$^{\Delta HBS}$ protected ADR-induced cardiac apoptosis by accelerating p53 degradation (Figs. 4 and 5). Interest in p53 posttranslational modifications and degradation increased dramatically, both during normal homeostasis and in ADR-induced responses [41,42]. For example, as a p53-specific E3 ubiquitin ligase, MDM2, is the principal cellular antagonist of p53, acting to limit the p53 growth-suppressive function [29,30]. Consistent with previous study, results from our study showed that the expression of MDM2 was inhibited and the expression of p53 was increased both in heart tissues and H9c2 cells treated with ADR [29], and we verified that FGF1$^{\Delta HBS}$ degraded p53 through promoting MDM2-mediated p53 ubiquitination (Figs. 6 and 7A). Another important post-transcriptional mechanism related to the inhibition of p53 is deacetylation, which is regulated by deacetylases. And as a kind of NAD-dependent deacetylase, Srit1/6/7 belongs to the sirtuin family widely existing in living organisms. Studies have shown that ADR can inhibit the expression of Sirt1/6/7 in renal podocyte cells [33]. Also, previous study has shown that increased expression of Sirt1/6/7 can reduce the expression of p53 protein and suppress p53 acetylation to improve heart and other organs diseases [32,34,35]. However, Sirt1, one of the most extensively studied members of its kind in histone deacetylase family to govern diverse cellular fates, is predominantly related to p53 activity. Indeed, the results from our study verified that FGF1$^{\Delta HBS}$ promoted p53 deacetylation by targeting Sirt1 rather than Sirt6 or Sirt7 in ADR-induced cardiotoxicity model (Figs. 6 & Fig. 7B–E & Fig. 8F–I). Given that acetylation and ubiquitylation of p53 occur on a similar set of lysine residues, thus they are mutually exclusive [37], when FGF1$^{\Delta HBS}$ promoted Sirt1-mediated p53 deacetylation, the deacetylation of p53 then facilitate MDM2-mediated p53 ubiquitination and consequent degradation. In addition, observed results in this study shown that the expression of Sirt6 and Sirt7 was reduced by ADR *in vitro* (Fig. 6B and Fig. S1) but not *in vivo* (Fig. 6A). These discrepancies may be attributed to different dose and duration of ADR administration [43].

An interesting finding of our study is that the cardioprotective effect of FGF1$^{\Delta HBS}$ against ADR-induced cardiotoxicity is independent of AMPK phosphorylation (Fig. S1 and Fig. S3A&B). As a cell-intrinsic regulator, AMPK plays a vital role in maintaining biological energy metabolism by modulating p53 activity [44,45]. AMPK activation induces phosphorylation of p53 on Ser15, and this activation promotes cellular survival in response to glucose deprivation [46]. However, study by Liu and colleagues reported that resveratrol protected against ADR-induced cardiomyocyte apoptosis by increasing AMPK phosphorylation to suppress the expression of p53 [47]. These controversial findings might be because of the diverse of metabolic procedure between proliferating mammalian cells and stress-induced cardiac injury as well as distinct chemicals (5-aminoimidazole-4-carboxamide riboside and resveratrol) for AMPK activation. Additionally, a recent study has reported increased expression of phosphorylated AMPK (p-AMPK) by FGF1$^{\Delta HBS}$ to maintain mitochondrial homeostasis and reduce oxidative stress in diabetic cardiomyopathy [48]. While, in the current study, we found FGF1$^{\Delta HBS}$ did not restore the decreased expression of p-AMPK induced by ADR *in vivo and in vitro* (Fig. S1 and Fig. S3A&B). These discrepancies between the reported data and our findings may be attributed to the fact that: (1) Two different disease models were applied, and (2) AMPK, an established metabolic stress sensor, has gained popularity in cardio-metabolic diseases rather than ADR-induced cardiotoxicity due to its powerful ability to control intracellular energy homeostasis in response to energetic stress.

The last thing to point out is that the putative cardioprotective strategies aimed to activate the FGF1-related pathways might become a promising potential treatment for ADR-induced cardiotoxicity.

Therefore, a number of natural extracts and clinical drugs [34,49–53] to active FGF1 could be screened to ameliorate heart damage caused by ADR, which provide the proof of translational studies designed to reduce adverse cardiovascular outcomes. More importantly, optimal cardioprotective strategies should not only interfere with the primary mechanisms of cardiotoxicity but enhance or at least preserve the antitumor capacity of ADR. Therefore, more studies will be required to fully dissect the effects of $FGF1^{\Delta HBS}$ on the efficacy of ADR-induced tumor killing.

In conclusion, we demonstrated here for the first time that $FGF1^{\Delta HBS}$ prevented myocardial injury in ADR-induced cardiotoxicity mouse model. Activation of Sirt1 by the non-mitogenic $FGF1^{\Delta HBS}$ greatly reduced p53 stability through increasing p53 deacetylation and subsequently promoting MDM2-mediated p53 ubiquitination and proteasome degradation to reverse cardiac oxidative damage and apoptosis, which protect myocardial remodeling and dysfunction against chemotherapy, as illustrated in Fig. 7G. Given the favorable metabolic activity and lower proliferative potential of $FGF1^{\Delta HBS}$ application, our data offer prospect that $FGF1^{\Delta HBS}$ may become a clinically useful agent for the treatment of ADR-induced cardiotoxicity.

Author's contribution

J.L.G. designed the study and supervised the project. M.J.X., Y.F.T., and J.W(a). performed experiments and drafted the manuscript. J.L.N., Z.F.H. and S.W.Y. provided experiment materials and participated in the part of Discussion. Z.Y.W., and Y.F.G. conducted *in vitro* experiments statistical analysis. G.P.L., J.W(b)., and J.H.L. conducted *in vivo* experiments statistical analysis. Q.B.L., T.G. and X.H.Z. helped with manuscript editing. All authors have approved the final version of the manuscript.

Declaration of competing interest

The authors declare no competing interests.

Acknowledgements

This study was supported by Qilu Young Scholar's Program of Shandong University (Grant No. 21330089963007). We thank Translational Medicine Core Facility of Shandong University for consultation and instrument availability that supported this work.

Appendix A. Supplementary data

Supplementary data to this article can be found online at https://doi.org/10.1016/j.redox.2021.102219.

References

[1] A.J. Wang, et al., Molecular mechanisms of doxorubicin-induced cardiotoxicity: novel roles of sirtuin 1-mediated signaling pathways, Cell. Mol. Life Sci. 78 (2021) 3105–3125, https://doi.org/10.1007/s00018-020-03729-y.
[2] X. Zhang, et al., FNDC5 alleviates oxidative stress and cardiomyocyte apoptosis in doxorubicin-induced cardiotoxicity via activating AKT, Cell Death Differ. 27 (2020) 540–555, https://doi.org/10.1038/s41418-019-0372-z.
[3] Y. Octavia, et al., Doxorubicin-induced cardiomyopathy: from molecular mechanisms to therapeutic strategies, J. Mol. Cell. Cardiol. 52 (2012) 1213–1225, https://doi.org/10.1016/j.yjmcc.2012.03.006.
[4] L. Zhao, et al., MicroRNA-140-5p aggravates doxorubicin-induced cardiotoxicity by promoting myocardial oxidative stress via targeting Nrf2 and Sirt2, Redox Biol. 15 (2018) 284–296, https://doi.org/10.1016/j.redox.2017.12.013.
[5] A.A. Belov, M. Mohammadi, Molecular mechanisms of fibroblast growth factor signaling in physiology and pathology, Cold Spring Harbor Perspect. Biol. 5 (2013), https://doi.org/10.1101/cshperspect.a015958.
[6] M. Xiao, et al., Regulatory role of endogenous and exogenous fibroblast growth factor 1 in the cardiovascular system and related diseases, Pharmacol. Res. 169 (2021), 105596, https://doi.org/10.1016/j.phrs.2021.105596.
[7] J.W. Jonker, et al., A PPARγ-FGF1 axis is required for adaptive adipose remodelling and metabolic homeostasis, Nature 485 (2012) 391–394, https://doi.org/10.1038/nature10998.
[8] J.M. Suh, et al., Endocrinization of FGF1 produces a neomorphic and potent insulin sensitizer, Nature 513 (2014) 436–439, https://doi.org/10.1038/nature13540.
[9] X. Wang, et al., FGF1 protects against APAP-induced hepatotoxicity via suppression of oxidative and endoplasmic reticulum stress, Clin. Res. Hepatol. Gastroenterol. 43 (2019) 707–714, https://doi.org/10.1016/j.clinre.2019.03.006.
[10] Y.Z. Zhao, et al., Prevent diabetic cardiomyopathy in diabetic rats by combined therapy of aFGF-loaded nanoparticles and ultrasound-targeted microbubble destruction technique, J. Contr. Release 223 (2016) 11–21, https://doi.org/10.1016/j.jconrel.2015.12.030.
[11] Y.Z. Zhao, et al., Improving the cardio protective effect of aFGF in ischemic myocardium with ultrasound-mediated cavitation of heparin modified microbubbles: preliminary experiment, J. Drug Target. 20 (2012) 623–631, https://doi.org/10.3109/1061186x.2012.702771.
[12] F.R. Formiga, et al., Controlled delivery of fibroblast growth factor-1 and neuregulin-1 from biodegradable microparticles promotes cardiac repair in a rat myocardial infarction model through activation of endogenous regeneration, J. Contr. Release 173 (2014) 132–139, https://doi.org/10.1016/j.jconrel.2013.10.034.
[13] L. Zheng, et al., Assessment of the preventive effect against diabetic cardiomyopathy of FGF1-loaded nanoliposomes combined with microbubble cavitation by ultrasound, Front. Pharmacol. 10 (2019) 1535, https://doi.org/10.3389/fphar.2019.01535.
[14] I.S. Babina, N.C. Turner, Advances and challenges in targeting FGFR signalling in cancer, Nat. Rev. Cancer 17 (2017) 318–332, https://doi.org/10.1038/nrc.2017.8.
[15] Z. Huang, et al., Uncoupling the mitogenic and metabolic functions of FGF1 by tuning FGF1-FGF receptor dimer stability, Cell Rep. 20 (2017) 1717–1728, https://doi.org/10.1016/j.celrep.2017.06.063.
[16] D. Wang, et al., FGF1(ΔHBS) ameliorates chronic kidney disease via PI3K/AKT mediated suppression of oxidative stress and inflammation, Cell Death Dis. 10 (2019) 464, https://doi.org/10.1038/s41419-019-1696-9.
[17] Q. Lin, et al., Activating adenosine monophosphate-activated protein kinase mediates fibroblast growth factor 1 protection from nonalcoholic fatty liver disease in mice, Hepatology 73 (2021) 2206–2222, https://doi.org/10.1002/hep.31568.
[18] J.C. Garbern, et al., Inhibition of mTOR signaling enhances maturation of cardiomyocytes derived from human-induced pluripotent stem cells via p53-induced quiescence, Circulation 141 (2020) 285–300, https://doi.org/10.1161/CIRCULATIONAHA.119.044205.
[19] J. Gu, et al., Inhibition of p53 prevents diabetic cardiomyopathy by preventing early-stage apoptosis and cell senescence, reduced glycolysis, and impaired angiogenesis, Cell Death Dis. 9 (2018) 82, https://doi.org/10.1038/s41419-017-0093-5.
[20] Y. Wang, et al., Inactivation of GSK-3beta by metallothionein prevents diabetes-related changes in cardiac energy metabolism, inflammation, nitrosative damage, and remodeling, Diabetes 58 (2009) 1391–1402, https://doi.org/10.2337/db08-1697.
[21] J. Gu, et al., Metallothionein is downstream of Nrf2 and partially mediates sulforaphane prevention of diabetic cardiomyopathy, Diabetes 66 (2017) 529–542, https://doi.org/10.2337/db15-1274.
[22] H. Yi, et al., A novel small molecule inhibitor of MDM2-p53 (APG-115) enhances radiosensitivity of gastric adenocarcinoma, J. Exp. Clin. Cancer Res. 37 (2018) 97, https://doi.org/10.1186/s13046-018-0765-8.
[23] C. Hu, et al., Osteocrin attenuates inflammation, oxidative stress, apoptosis, and cardiac dysfunction in doxorubicin-induced cardiotoxicity, Clin. Transl. Med. 10 (2020) e124, https://doi.org/10.1002/ctm2.124.
[24] X.Q. Tian, et al., Prevention of doxorubicin-induced cardiomyopathy using targeted MaFGF mediated by nanoparticles combined with ultrasound-targeted MB destruction, Int. J. Nanomed. 12 (2017) 7103–7119, https://doi.org/10.2147/ijn.S145799.
[25] X. Hu, et al., miR-200a attenuated doxorubicin-induced cardiotoxicity through upregulation of Nrf2 in mice, Oxid. Med. Cell. Longev. 2019 (2019), 1512326, https://doi.org/10.1155/2019/1512326.
[26] H. Men, et al., The regulatory roles of p53 in cardiovascular health and disease, Cell. Mol. Life Sci. 78 (2021) 2001–2018, https://doi.org/10.1007/s00018-020-03694-6.
[27] S. Wang, P. Song, M.H. Zou, Inhibition of AMP-activated protein kinase α (AMPKα) by doxorubicin accentuates genotoxic stress and cell death in mouse embryonic fibroblasts and cardiomyocytes: role of p53 and SIRT1, J. Biol. Chem. 287 (2012) 8001–8012, https://doi.org/10.1074/jbc.M111.315812.
[28] P. Secchiero, et al., Activation of the p53 pathway down-regulates the osteoprotegerin expression and release by vascular endothelial cells, Blood 111 (2008) 1287–1294, https://doi.org/10.1182/blood-2007-05-092031.
[29] F. Xu, et al., Effects of Ganoderma lucidum polysaccharides against doxorubicin-induced cardiotoxicity, Biomed. Pharmacother. 95 (2017) 504–512, https://doi.org/10.1016/j.biopha.2017.08.118.
[30] X. Liu, et al., Pifithrin-alpha protects against doxorubicin-induced apoptosis and acute cardiotoxicity in mice, Am. J. Physiol. Heart Circ. Physiol. 286 (2004) H933–H939, https://doi.org/10.1152/ajpheart.00759.2003.
[31] S. Matsushima, J. Sadoshima, The role of sirtuins in cardiac disease, Am. J. Physiol. Heart Circ. Physiol. 309 (2015) H1375–H1389, https://doi.org/10.1152/ajpheart.00053.2015.
[32] M. Wood, et al., Trichostatin A inhibits deacetylation of histone H3 and p53 by SIRT6, Arch. Biochem. Biophys. 638 (2018) 8–17, https://doi.org/10.1016/j.abb.2017.12.009.
[33] M. Liu, et al., Sirt6 deficiency exacerbates podocyte injury and proteinuria through targeting Notch signaling, Nat. Commun. 8 (2017) 413, https://doi.org/10.1038/s41467-017-00498-4.

[34] C. Zhang, et al., Resveratrol attenuates doxorubicin-induced cardiomyocyte apoptosis in mice through SIRT1-mediated deacetylation of p53, Cardiovasc. Res. 90 (2011) 538–545, https://doi.org/10.1093/cvr/cvr022.
[35] O. Vakhrusheva, et al., Sirt7 increases stress resistance of cardiomyocytes and prevents apoptosis and inflammatory cardiomyopathy in mice, Circ. Res. 102 (2008) 703–710, https://doi.org/10.1161/CIRCRESAHA.107.164558.
[36] C.L. Brooks, W. Gu, Ubiquitination, phosphorylation and acetylation: the molecular basis for p53 regulation, Curr. Opin. Cell Biol. 15 (2003) 164–171, https://doi.org/10.1016/s0955-0674(03)00003-6.
[37] Q. Zhang, et al., A small molecule Inauhzin inhibits SIRT1 activity and suppresses tumour growth through activation of p53, EMBO Mol. Med. 4 (2012) 298–312, https://doi.org/10.1002/emmm.201100211.
[38] R.M. Damiani, et al., Pathways of cardiac toxicity: comparison between chemotherapeutic drugs doxorubicin and mitoxantrone, Arch. Toxicol. 90 (2016) 2063–2076, https://doi.org/10.1007/s00204-016-1759-y.
[39] C. Tonelli, I.I.C. Chio, D.A. Tuveson, Transcriptional regulation by Nrf2, Antioxidants Redox Signal. 29 (2018) 1727–1745, https://doi.org/10.1089/ars.2017.7342.
[40] P. Singh, et al., Sulforaphane protects the heart from doxorubicin-induced toxicity, Free Radic. Biol. Med. 86 (2015) 90–101, https://doi.org/10.1016/j.freeradbiomed.2015.05.028.
[41] J. Liu, et al., UFMylation maintains tumour suppressor p53 stability by antagonizing its ubiquitination, Nat. Cell Biol. 22 (2020) 1056–1063, https://doi.org/10.1038/s41556-020-0559-z.
[42] V. Lang, et al., Analysis of defective protein ubiquitylation associated to adriamycin resistant cells, Cell Cycle 16 (2017) 2337–2344, https://doi.org/10.1080/15384101.2017.1387694.
[43] D. Han, et al., The tumor-suppressive human circular RNA CircITCH sponges miR-330-5p to ameliorate doxorubicin-induced cardiotoxicity through upregulating SIRT6, survivin, and SERCA2a, Circ. Res. 127 (2020) e108–e125, https://doi.org/10.1161/CIRCRESAHA.119.316061.
[44] D. Carling, AMPK signalling in health and disease, Curr. Opin. Cell Biol. 45 (2017) 31–37, https://doi.org/10.1016/j.ceb.2017.01.005.
[45] C.W. Lee, et al., AMPK promotes p53 acetylation via phosphorylation and inactivation of SIRT1 in liver cancer cells, Cancer Res. 72 (2012) 4394–4404, https://doi.org/10.1158/0008-5472.Can-12-0429.
[46] R.G. Jones, et al., AMP-activated protein kinase induces a p53-dependent metabolic checkpoint, Mol Cell 18 (2005) 283–293, https://doi.org/10.1016/j.molcel.2005.03.027.
[47] M.H. Liu, et al., Resveratrol protects cardiomyocytes from doxorubicin-induced apoptosis through the AMPK/P53 pathway, Mol. Med. Rep. 13 (2016) 1281–1286, https://doi.org/10.3892/mmr.2015.4665.
[48] D. Wang, et al., FGF1(DeltaHBS) prevents diabetic cardiomyopathy by maintaining mitochondrial homeostasis and reducing oxidative stress via AMPK/Nur77 suppression, Signal Transduct. Target Ther. 6 (2021) 133, https://doi.org/10.1038/s41392-021-00542-2.
[49] D. Liu, et al., PGC1alpha activation by pterostilbene ameliorates acute doxorubicin cardiotoxicity by reducing oxidative stress via enhancing AMPK and SIRT1 cascades, Aging (Albany NY) 11 (2019) 10061–10073, https://doi.org/10.18632/aging.102418.
[50] Y.Z. Wu, et al., Berberine ameliorates doxorubicin-induced cardiotoxicity via a SIRT1/p66Shc-mediated pathway, Oxid. Med. Cell. Longev. 2019 (2019), 2150394, https://doi.org/10.1155/2019/2150394.
[51] Z. Sun, et al., Dihydromyricetin alleviates doxorubicin-induced cardiotoxicity by inhibiting NLRP3 inflammasome through activation of SIRT1, Biochem. Pharmacol. 175 (2020), 113888, https://doi.org/10.1016/j.bcp.2020.113888.
[52] J. Zhai, et al., Calycosin ameliorates doxorubicin-induced cardiotoxicity by suppressing oxidative stress and inflammation via the sirtuin 1-NOD-like receptor protein 3 pathway, Phytother Res. 34 (2020) 649–659, https://doi.org/10.1002/ptr.6557.
[53] V. Quagliariello, et al., The SGLT-2 inhibitor empagliflozin improves myocardial strain, reduces cardiac fibrosis and pro-inflammatory cytokines in non-diabetic mice treated with doxorubicin, Cardiovasc. Diabetol. 20 (2021) 150, https://doi.org/10.1186/s12933-021-01346-y.